Generalized oscillator strengths of the hydrogen-molecule ion

Mineo Kimura
Argonne National Laboratory, Argonne, Illinois 60439
and Rice University, Houston, Texas 77251
(Received 8 January 1987)

The generalized oscillator strength (GOS) of H_2^+ is calculated comprehensively for both discrete-discrete and discrete-continuum transitions using exact Born-Oppenheimer wave functions. The calculation presumes the Born-Oppenheimer separation, and thus gives the GOS dependence upon the internuclear distance and the angle between the molecular axis and the momentum transfer, in addition to the dependence upon the energy and momentum-transfer magnitude. The theoretical study of the molecular GOS is extremely rare even for discrete excitation and is virtually absent for continuum transitions. The present study serves as a guideline for full understanding of the molecular GOS in general, although no experimental results on the key aspect, i.e., the dependence of the GOS upon the momentum transfer, are available for comparison with theory.

I. INTRODUCTION

All information about any inelastic collision of a high-energy charged particle is embedded in a target property, i.e., the generalized oscillator strength (GOS), within the framework of the first Born representation. In particular, the essential part of differential, as well as total cross sections, are indeed determined by the GOS. Hence, the understanding of characteristics of the GOS directly connects to that of collision dynamics.[1,2] Since the historic work on the GOS by Bethe,[3,4] theoretical study of the GOS has concentrated predominantly on discrete transitions in atomic systems.[1] Furthermore, for continuum transitions, treatments have been limited to atomic hydrogen[5,6] or to central-field models of atoms,[7] owing clearly to the difficulty of obtaining more accurate wave functions to describe continuum states. Although knowledge of the GOS for molecules is more urgently necessary in various applications, the study of the molecular GOS is relatively limited.[8] In addition, to the best of my knowledge, virtually no detailed study has been reported on the molecular GOS which involves continuum states. I have conducted a systematic and comprehensive study of the molecular GOS for discrete, as well as continuum, transitions for the H_2^+ system for the first time. Although this study of the molecular GOS for one-electron diatomic molecular (OEDM) systems may appear somewhat academic because relevant experiments on H_2^+, e.g., measurements of the angular distribution of inelastically scattered electrons are not feasible at present; it is, however, a necessary step toward full elucidation of the molecular GOS in general. Taking full advantage of the knowledge of exact wave functions, both for discrete and continuum states of OEDM systems,[9–11] one can explore characteristics of the molecular GOS without any ambiguity.

Previously, Peek[12] has investigated the molecular GOS for the H_2^+ system for several lower discrete states. Since the main focus of his study lay on electron-impact dissociation of the H_2^+ via unbound discrete channels ($2p\sigma_u$, $2p\pi_u$, and $2s\sigma_g$ states in the united-atom designation), his discussion of the molecular GOS is brief and most discussion apparently concentrates on the dissociation cross section.

As is now well known from experiments and from the general consideration,[1] a large part of the GOS comes from continuum transitions or ionizations. Therefore, discussion of the molecular GOS of continuum transition should be included for full understanding of the GOS. The primary purpose of the present report is the following: (i) To illustrate results of the GOS of H_2^+ both for discrete and continuum transitions calculated by using *exact* Born-Oppenheimer wave functions for both states, and (ii) to discuss characteristics of the molecular GOS in each transition in conjunction with that for the H atom and the He^+ atomic ion as two extremes of H_2^+ molecular ion.

II. DEFINITIONS

Sets of the coordinate system for H_2^+ are shown in Fig. 1. Note that the orientation of molecular axis with

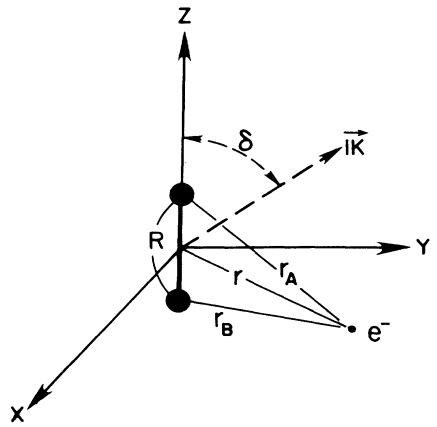

FIG. 1. Sets of coordinate system of H_2^+ and momentum transfer K.

respect to momentum transfer K is shown by angle δ in Fig. 1. Atomic units are used throughout.

A. The generalized oscillator strength

The generalized oscillator strength $f_n(K,R)$ for transition of one-electron diatomic molecular system from its ground state to discrete or continuum states is defined as (see, for example, Ref. 1)

$$f_n(K,R)=\frac{2E_n}{K^2}\,|\,\epsilon_n(K,R)\,|^2 \tag{1}$$

with

$$|\,\epsilon_n(K,R)\,|^2=\int_0^{\pi}|\,\epsilon_n(K,R,\delta)\,|^2(\sin\delta)d\delta/2 \tag{2}$$

and

$$\epsilon_n(K,R,\delta)=\int_0^{\infty}\phi_n^{\mathrm{BO}}(\mathbf{r},R)e^{i\mathbf{K}\cdot\mathbf{r}}\phi_0^{\mathrm{BO}}(\mathbf{r},R)d\mathbf{r}\ , \tag{3}$$

where $\epsilon_n(K,R)$, is the so-called scattering form factor, $\mathbf{K}$ represents momentum transfer $\mathbf{K}=\mathbf{k}_0-\mathbf{k}_n$, $\mathbf{k}_0$ is the momentum of an incident particle before the collision, and $\mathbf{k}_n$ that after the collision. The symbol $\phi_n^{\mathrm{BO}}(\mathbf{r},R)$ represents the Born-Oppenheimer (BO) wave function for the nth excited state, and $\phi_0^{\mathrm{BO}}(\mathbf{r},R)$ that for the ground state. The symbol E_n represents the excitation energy of the nth state measured from the ground state.

Using the GOS in Eq. (1), the differential, as well as the total, cross sections are readily derived within the first Born approximation. For an electron collision, the differential cross section can be written

$$\frac{d\sigma}{d\Omega}=4\left[\frac{k_n}{k_0}\right]\frac{1}{K^4}\times[\,|\,\langle X_n(R)\,|\,\epsilon_n(K,R)\,|\,X_0(R)\rangle_R\,|^2]\ , \tag{4}$$

where $X_i(R)$ represents the nuclear vibrational wave function. $\langle\cdots\rangle_R$ denotes integration over the internuclear separation R. Correspondingly, the total cross section is

$$\sigma=\frac{2\pi}{k_0^2}\int_{k_n-k_0}^{k_n+k_0}|\,\langle X_n(R)\,|\,\epsilon_n(K,R)\,|\,X_0(R)\rangle_R\,|^2\frac{dK}{K^3}\ . \tag{5}$$

In the derivation of Eqs. (4) and (5), certain simplifying assumptions are made. First, the coupling between vibrational and rotational states is disregarded. Second, the slight dependence of the momentum transfer upon the rotational quantum numbers of the initial and final states is disregarded. Further, the rotational motion is extremely slow compared to the electronic excitation and may be treated adiabatically. Thus, the average over the initial rotational states and the summation over the final rotational states may be effectively replaced by the integration over the angle δ as indicated in Eq. (2). For further details, see Ref. 2 and Sec. 3.5 of Ref. 1. As clearly seen from Eqs. (4) and (5), the GOS constitutes the central object of both cross sections, and thereby, its study is precisely nothing but a detailed study of collision dynamics. General features of the GOS and of the form factor are given in Ref. 1.

B. The Born-Oppenheimer molecular eigenstates

Exact molecular eigenstates and eigenvalues for discrete and continuum states were generated[9–11] using the prolate spheroidal coordinates (ξ,η,ϕ), which make the Schrödinger equation separable. The solutions may be expressed in the form

$$\phi_i^{\mathrm{BO}}(\mathbf{r},R)=(2\pi)^{-1/2}X(\xi)S(\eta)\exp(im\phi)\ . \tag{6}$$

For discrete states, one may write

$$X(\xi)=(\xi^2-1)^{|m|/2}e^{-c\xi}(\xi+1)^{\sigma}\sum_j c_j\left[\frac{\xi-1}{\xi+1}\right]^j, \tag{7a}$$

$$S(\eta)=\sum_l f_l P_l^{|m|}(\eta)\ , \tag{7b}$$

using the symbols defined in Ref. 9. For continuum states,[10,11] one may write

$$X(\xi)=\left[\frac{\xi-1}{\xi+1}\right]^{|m|/2}F(\xi)\ , \tag{8}$$

and $F(\xi)$ satisfies the differential equation

$$(\xi^2-1)F''(\xi)+(2\,|\,m\,|+\xi)F'(\xi)+(d^2\xi^2+q\xi-A)F(\xi)=0\ , \tag{9}$$

$F(\xi)$ being obtained numerically by integration of Eq. (9). Similarly, one may put

$$S(\eta)=\sum_l d_l P_l^{|m|}(\eta)\ . \tag{10}$$

The continuum wave functions are normalized to include the density of continuum states.

Now, Eq. (3) can be reduced in numerically tractable form using the BO wave functions (7)—(10) as

$$\epsilon(K,R,\delta)=\left[\frac{R}{2}\right]^3\int_1^{\infty}d\xi\int_{-1}^{1}d\eta(\xi^2-\eta^2)\times\exp\left[\frac{iKR}{2}\xi\eta\cos\delta\right]J_{|m_1-m_2|}\times\left[\frac{KR}{2}(\xi^2-1)^{1/2}(1-\eta^2)^{1/2}\sin\delta\right]\times X_n(\xi)X_0(\xi)S_n(\eta)S_0(\eta)\ , \tag{11}$$

where $J_m(X)$ represents the Bessel function. The 28-point Gauss-Laguerre and 32-point Gauss-Legendre quadratures have been found to be adequate to evaluate nonseparable double integrals in Eq. (3) with relative errors less than 1×10^{-6}. The Simpson method was used to integrate over angle δ in Eq. (2) with relative errors less than 1×10^{-4}.

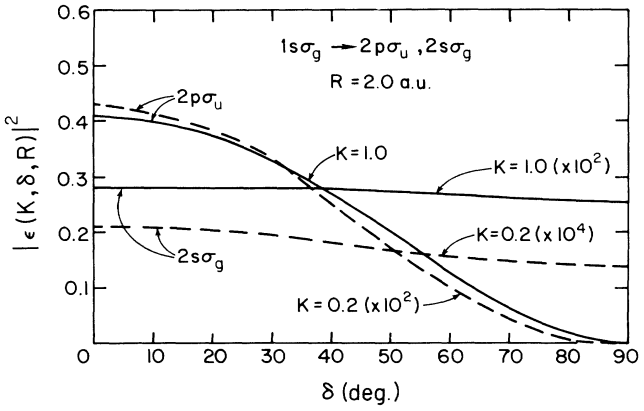

FIG. 2. $|\epsilon(K,R,\delta)|^2/K^2$ vs orientation angle δ for $1s\sigma_g \rightarrow 2p\sigma_u$ and $2s\sigma_g$ transitions with various values of K.

III. RESULTS AND DISCUSSIONS

A. Discrete-discrete GOS

The dependence of the form factor on the angle δ for $1s\sigma_g \rightarrow 2p\sigma_u$ and $1s\sigma_g \rightarrow 2s\sigma_g$ transitions at fixed $R=2.0$ a.u. is shown on Fig. 2. As is observed by expanding Eq. (11) with the help of Eqs. (6)—(10) in a power series of the exponential, certain form factors vanish identically for a specific value of δ. As is apparent from the figure, for the $np\sigma_u$ final state, $|\epsilon(K,R)|^2$ is zero at $\delta=\pi/2$, while it goes to zero at $\delta=0$ for the $np\pi_u$ final state. $|\epsilon(K,R)|^2$ is nonzero for all angles for the $ns\sigma_g$ state. Although the magnitude of the form factor varies significantly depending upon the magnitude of the momentum transfer K, its shape as a function of δ is very similar to each other. At small K for the $1s\sigma_g \rightarrow 2p\sigma_u$ transition, $\epsilon(K,R)$ approaches the cosine curve, while it starts deviating from the cosine curve having larger magnitudes at larger δ at large K.

Figure 3 displays $|\epsilon(K,R)|^2/K^2$ versus $\ln(Ka_0)^2$ at various R values for the $1s\sigma_g \rightarrow 2s\sigma_g$ transition. Note that $1s\sigma_g$ and $2s\sigma_g$ molecular states correspond to $He^+(1s)$ and $He^+(2s)$ at $R \rightarrow 0$, and $H^+ + H(1s)$ and $H^+ + H(2s+2p_0)$ at $R \rightarrow \infty$, respectively. Therefore, the present result should tie to each atomic GOS at these two asymptotic regions. Indeed, results clearly show that as R increases, the magnitude of the GOS at small momentum transfer K increases indicating that the molecular GOS approaches the $H(n=2)$ GOS,[6] while the present result becomes close the $He^+(2s)$ GOS as R decreases which corresponds to optically forbidden transition.

Similar results for the $1s\sigma_g \rightarrow 2p\sigma_u$ transition are seen in Fig. 4. There is a decisive difference from the earlier case. That is to say, the $1s\sigma_g$ and $2p\sigma_u$ states are degenerate asymptotically forming $H^+ + H(1s)$ channel, although these states correspond to different states, $He^+(1s)$ and $He^+(n=2)$, at $R=0$, respectively. This $1s\sigma_g \rightarrow 2p\sigma_u$ transition is a special additional process possible in only homonuclear molecules, but not in atoms as was first pointed out by Kołos[8(a)] in reference to the hydrogen molecule. As is apparent from Fig. 4, $|\epsilon(K,R)|^2/K^2$ seems to increase as internuclear separation R becomes larger, although the GOS for this transition itself approaches zero as R increases because of an energy defect between these states [see, Eq. (1)]. This certainly reflects the fact that there is no transition between the same states. Simple analysis of this characteristic using a linear combination of atomic orbitals (LCAO) method reveals that for large R with fixed K, $\epsilon(K,R)$ behaves like

$$\sin\left[\frac{\mathbf{K}\cdot\mathbf{R}}{2}\right],$$

while $\epsilon(K,R)$ is roughly linearly dependent to R for small R with fixed K. Needless to say, in the limit of $K \rightarrow 0$, the GOS of this transition approaches the optical oscillator strength between corresponding states of He^+ ion

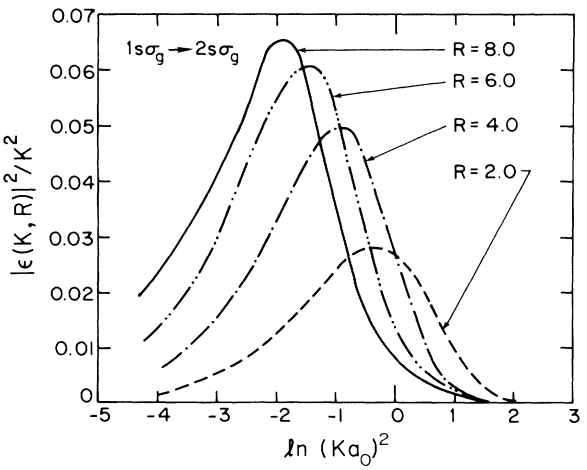

FIG. 3. $|\epsilon(K,R)|^2/K^2$ vs $\ln(Ka_0)^2$ for $1s\sigma_g \rightarrow 2s\sigma_g$ transition with different internuclear separation R.

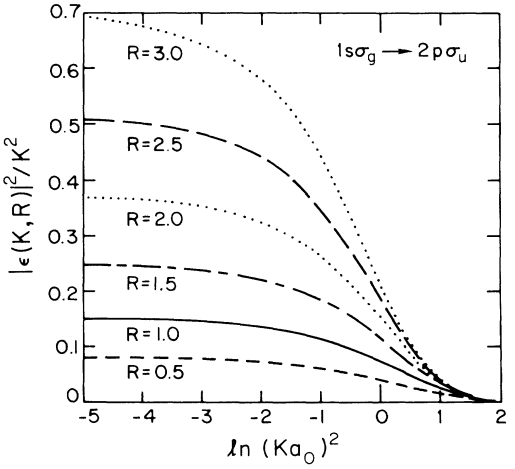

FIG. 4. $|\epsilon(K,R)|^2/K^2$ vs $\ln(Ka_0)^2$ for $1s\sigma_g \rightarrow 2p\sigma_u$ transition with different R.

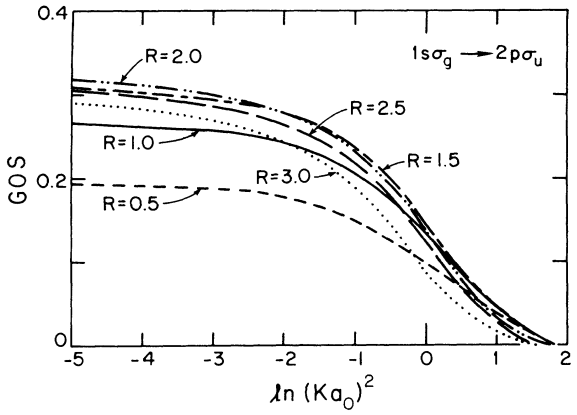

FIG. 5. The molecular GOS vs $\ln(Ka_0)^2$ for $1s\sigma_g \rightarrow 2p\sigma_u$ transition for changing R value.

since the $1s\sigma_g \rightarrow 2p\sigma_u$ transition is an optically allowed transition.

The GOS for the $1s\sigma_g \rightarrow 2p\sigma_u$ transition as a function of R is shown in Fig. 5. Interestingly, the GOS at $R=2.0$ a.u., i.e., the equilibrium distance of H_2^+, possesses the largest magnitude in the region of $K \lesssim 0.6$ compared to others calculated by different R. And in both sides of R departing from $R=2.0$ a.u., its magnitude decreases, although the rate of decrease is less drastic for larger R side.

The $|\epsilon(K,R)|^2/K^2$ for the $1s\sigma_g \rightarrow 3p\sigma_u$ transition is shown on Fig. 6 as a function of $\ln(Ka_0)^2$. Two interesting features are apparent in the figure: (i) the GOS possesses a minimum as K varies for cases in $R \geq 4.0$ a.u. (no minimum is observed for the GOS in $R \leq 2.0$ a.u. for entire K values), and (ii) the GOS approaches a finite value as $K \rightarrow 0$ (optical limit) since this transition is optically allowed. The occurrence of a minimum in the GOS at fixed R is attributable to the similar reason as for that of atomic GOS or the Cooper minimum for the photoabsorption cross section. Any $1s\sigma_g \rightarrow nl\sigma_u$ series transition shares the same trends mentioned above, namely, the GOS having a minimum as K varies and a finite value at

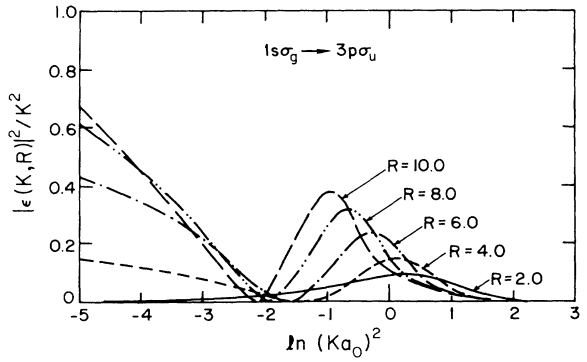

FIG. 6. $|\epsilon(K,R)|^2/K^2$ vs $\ln(Ka_0)^2$ for $1s\sigma_g \rightarrow 3p\sigma_u$ transition for different R value.

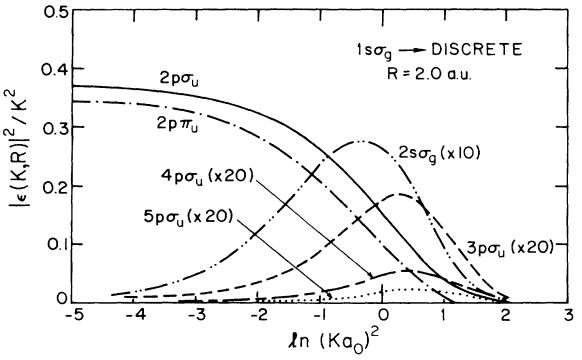

FIG. 7. $|\epsilon(K,R)|^2/K^2$ vs $\ln(Ka_0)^2$ for $1s\sigma_g \rightarrow$ various discrete transitions at fixed $R=2.0$ a.u.

$K \rightarrow 0$, except for the $1s\sigma_g \rightarrow 2p\sigma_n$ transition. Again, the $2p\sigma_u$ is the special state appearing only in a homonuclear molecule and hence, possesses unique molecular character compared to the other states which belong to the $nl\sigma_u$ family.

As a summary of this subsection, several results of $|\epsilon(K,R)|^2/K^2$ from the ground state to several excited states at $R=2.0$ a.u. (equilibrium distance) are illustrated in Fig. 7. Again, the excitation energy must be multiplied to obtain the actual GOS from the quantity shown in the figure. Therefore, the actual difference of the magnitude in the GOS for $np\sigma_u$ transition series becomes somewhat smaller compared to ones in Fig. 7. However, the general trend of the same l series is well illustrated in the figure.

B. Discrete-continuum GOS

Similarly to Fig. 2, the δ dependence on $|\epsilon(K,R,\epsilon_j)|^2$ from the discrete ground state $1s\sigma_g$ to $l=0$ and 1 continuum states with ejected electron energy $\epsilon_j=1$ a.u. at $R=2.0$ a.u. is displayed in Fig. 8. Remarkable differences found in the present figure from discrete-discrete transitions are that any $|\epsilon(K,R,\epsilon_j)|^2/K^2$ starts very small

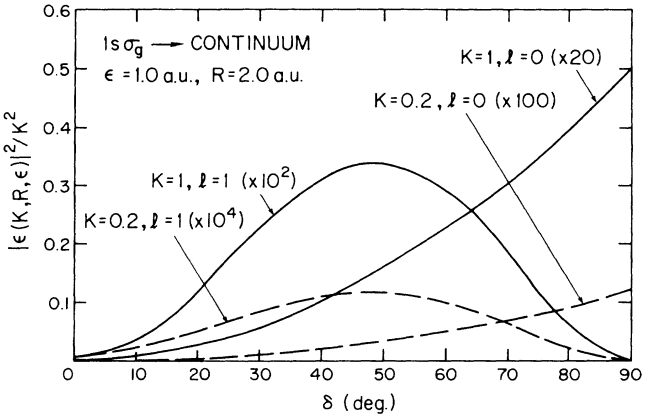

FIG. 8. $|\epsilon(K,R,\delta,\epsilon)|^2/K^2$ vs orientation angle δ for $1s\sigma_g \rightarrow |\epsilon,l,m=0\rangle$ continuum transition at fixed $R=2.0$ a.u.

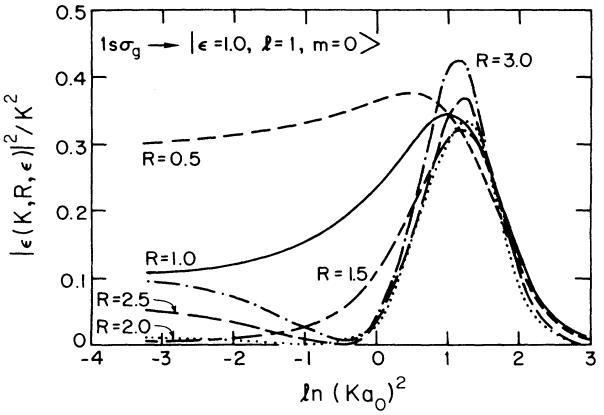

FIG. 9. $|\epsilon(K,R,\epsilon)|^2/K^2$ vs $\ln(Ka_0)^2$ for $1s\sigma_g \rightarrow |\epsilon=1.0, l=1, m=0\rangle$ continuum transition with R changing.

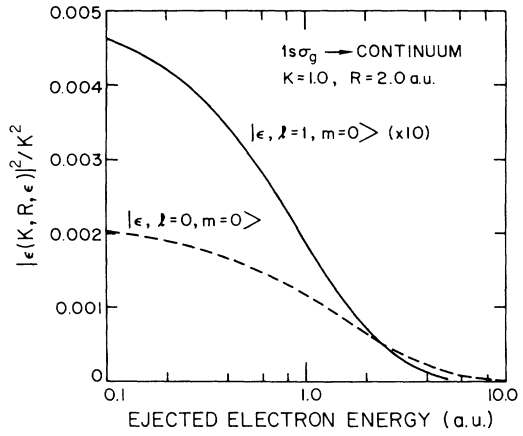

FIG. 11. $|\epsilon(K,R,\epsilon)|^2/K^2$ vs ejected electron energy ϵ for $1s\sigma_g \rightarrow |\epsilon, l=0, m=0\rangle$ and $|\epsilon, l=1, m=0\rangle$ transitions at $K=1.0$ and $R=2.0$ a.u.

value at angle $\delta=0$ for the $1s\sigma_g \rightarrow$continuum transition with subsequent growing as angle δ increases and there is a maximum around $\delta\simeq 50°$ for the $1s\sigma_g$-$\epsilon_j p\sigma_u$ transition, although they behave similarly to that of counterparts in discrete-discrete transition at larger angles. Although only $l=0,1$, cases are shown, obviously, due to symmetric nature in the molecular wave function used, $\epsilon(K,R,\epsilon_j)$ obtained from even-l or odd-l continuum states shares similar characteristic features in shape. The R dependence of $|\epsilon(K,R,\epsilon_j)|^2/K^2$ to the $1s\sigma_g \rightarrow \epsilon_j p\sigma_u$ transition at ejected electron energy $\epsilon_j=1.0$ a.u. is shown in Fig. 9. Two features observed should be particularly stressed: (i) the so-called Bethe ridge[1] develops noticeably as R increases, and (ii) the presence of a minimum around $K\sim 0.8$, similar to the ones seen in Fig. 6 for the $1s\sigma_g \rightarrow 3p\sigma_u$ transitions, becomes marked when $R=2.0$ a.u. and up. As has been seen in discrete-discrete transition, the shape of the GOS at small R resembles that of the He^+ ion, while as R increases it becomes closer to that of the H atom, as expected. The well-known property that $|\epsilon(K,R,\epsilon_j)|^2/K^2$ has a sharp maximum around $(Ka_0)^2=E$ (the Bethe ridge) is quite evident in the figure.

Figure 10 shows $|\epsilon(K,R,\epsilon_j)|^2/K^2$ for different partial wave l's at fixed $R=2.0$ a.u. One sees a gradual decrease of magnitude as l increases with giving even-l cases larger values compared to that of odd-l cases. Note that only the $l=1$ ($\epsilon_j p\sigma_u$) case exhibits a noticeable minimum in the GOS within the K ranges studied.

Figure 11 shows $|\epsilon(K,R,\epsilon_j)|^2/K^2$ versus ejected electron energy ϵ_j at fixed $K=1.0$ and $R=2.0$ a.u. The ϵ_j dependence of the shape is quite similar to each other regardless of the l value. Contribution from $\epsilon_j=1$ a.u. and below to the molecular GOS constitutes more than 95% of the total under conditions considered.

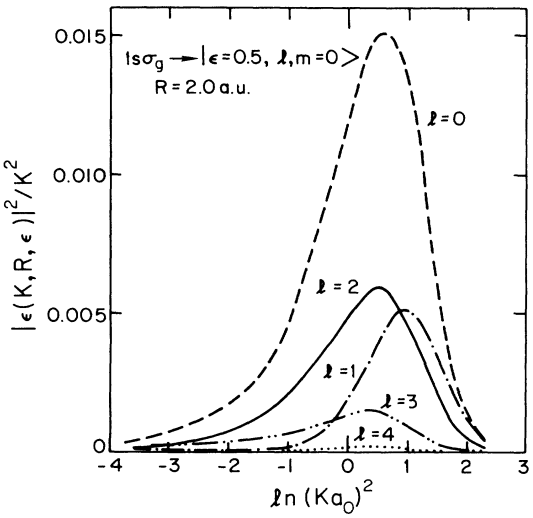

FIG. 10. $|\epsilon(K,R,\epsilon)|^2/K^2$ vs $\ln(Ka_0)^2$ for $1s\sigma_g \rightarrow |\epsilon=0.5, l, m=0\rangle$ continuum transition at fixed $R=2.0$ a.u.

C. The sum rule and the mean excitation energy

The moment of the μth order of the distribution of the GOS is defined[1] by

$$S(\mu)=\int \frac{df}{dE}E^{\mu}dE\ , \tag{12}$$

and its derivative with respect to the order μ is

$$L(\mu)=\frac{dS(\mu)}{d\mu}=\int \frac{df}{dE}E^{\mu}\ln E\, dE\ . \tag{13}$$

The integrals are taken over all continua as well as includ-

TABLE I. Representative results of the sum rule. The sum rule for arbitrarily chosen δ and K at fixed $R=2.0$ a.u.

	$K=0.5$		$K=1.0$	
Transition	$\delta=0°$	$\delta=45°$	$\delta=0°$	$\delta=45°$
Discrete	0.78	0.83	0.51	0.53
Continuum	0.21	0.17	0.48	0.46
Total	0.99	1.0	0.99	0.99

TABLE II. Representative results of the sum rule. The sum rule integrated over angle δ with $K=0$ (optical limit).

R (a.u.)	Transition		
	Discrete	Continuum	Total
1.0	0.782	0.216	0.998
2.0	0.865	0.133	0.998
4.0	0.803	0.196	0.999
⋮			
∞	0.565	0.435	1.00

ed in the summation over all excited states. The mean excitation energies $I(\mu)$, defined by

$$\ln I(\mu)=L(\mu)/S(\mu) \tag{14}$$

are crucial to many properties of atoms and molecules.[1] In the present work, we restrict our discussion specifically to investigate $\mu=0$ case only. When $\mu=0$, $I(0)$ is the Bethe excitation energy for stopping power.[1] Making use of the previous results for the H_2^+ GOS's, the sum rule and the mean excitation energy have been evaluated. Those results are tabulated in Tables I and II for the sum rule, and displayed in Fig. 12 for the mean excitation energy. As seen from Table I, *the sum rule is clearly satisfied independently for each fixed K, R, and δ.* This is mathematically provable following the procedure described in Ref. 13. Note that as the momentum transfer K increases, a contribution from continuum states to the sum rule expectedly increases.

The sum rule integrated over δ with $K=0$ (optical limit) shows in Table II that a contribution from discrete transitions to the total of the sum rule is the largest (87%) when $R=2.0$ a.u. It decreases smoothly as R increases approaching to 57% of the H atom[6] at $R\rightarrow\infty$. It also decreases as R decreases approaching to again 57% of the He^+ ion. [Note that the ratio of the continuum contribution to the discrete contribution to $S(0)$ in a hydrogenlike ion is independent of the nuclear charge.] A contribution of the $2p\sigma_u$ state to the sum rule at $R=2.0$ a.u. has about 37% with 93% of the total coming from joint $(2p\sigma_u+2p\pi_u)$ contribution to whole discrete transitions. As repeatedly discussed above, the $2p\sigma_u$ is the special extra state appearing only in homonuclear molecule, and it is interesting to see a role of this state in the GOS in conjunction with understanding collision dynamics.

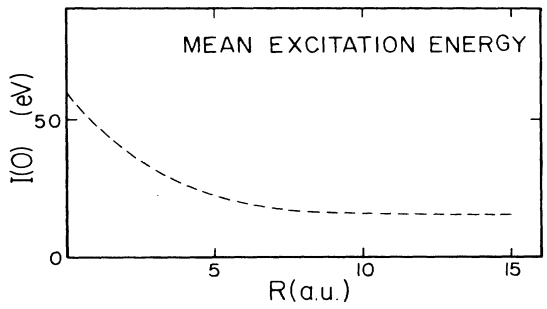

FIG. 12. The mean excitation energy as a function of R.

The mean excitation energy (MEE) varies smoothly as a function of R as shown in Fig. 12. Chiefly owing to the increasing role of the $2p\sigma_u$ state, the MEE gradually becomes larger from that of the hydrogen atom 15 eV at $R\rightarrow\infty$ to that of the He^+ atom, 60 eV, at $R\rightarrow 0$, although the value of the MEE increases rather drastically at smaller $R\lesssim 5$ a.u. to reach that of the He^+ ion at the united-atom limit.

IV. CONCLUSIONS

Important characteristic features of molecular form factors and molecular GOS's for both discrete-discrete and discrete-continuum transitions in the H_2^+ system found in the present study are summarized: (i) Presence of a marked minimum in the GOS for both discrete-discrete and discrete-continuum transitions as R changes has been found for the first time. This minimum is analogous to the one frequently found in atomic GOS[1] (as a function of K^2) and, similarly, to the one in the optical limit known as the Cooper minimum in the photoabsorption cross section as a function of photon energy. (ii) Special states (for example, the $2p\sigma_u$ state), which arise only from molecular formation and have no analogs in an atom, play an important role for full understanding of general properties related to the GOS and also collision dynamics. As an illustration, a dominant contribution to discrete portion of the distribution of the GOS comes from the $2p\sigma_u$ transition. (iii) The sum rule, viz.,

$$\int \frac{df(K,R,\delta,\epsilon)}{d\epsilon}d\epsilon=1\ ,$$

is valid independently for each fixed K, R, and δ. This result also implies that the derivative of $df(K,R,\delta,\epsilon)/d\epsilon$ with respect to K, R, or δ sums up to zero. The derivative with respect to K has been discussed already.[14,15] However, the remark on the derivative with respect to R and δ is new. This property specific to the molecular GOS may have useful applications in data analysis. A contribution from discrete transitions to the sum rule occupies more than 87% of the total integrated over K and δ at internuclear separation $R=2.0$ a.u. (equilibrium distance). As R increases, partitioning of the sum rule slowly approaches to that of the hydrogen atom in which 57% of the total is accounted for discrete transitions. (iv) Generally, the GOS for both discrete and continuum transitions is a sensitive function of R, δ, and ϵ_j (for continuum transition only). (v) The mean excitation energy of the H_2^+ is a smooth function of R, connecting that of He^+ ion and H atom at two extremes of R. Note that, for a hydrogenlike atomic ion of nuclear charge Z, $I(0)=Z^2\exp(0.096982)/2$ a.u. $=15.0Z^2$ eV.

Lastly, it would be extremely interesting if coincidence measurement of the state selected differential cross section for collision of electron with the H_2^+ molecular ion at fixed R is able to be carried out, since result from this kind of study provides comprehensive and detailed insight of collision dynamics which also serves stringent test for theoretical approach such as the present one.

ACKNOWLEDGMENTS

Stimulating discussions with Dr. M. Inokuti and Dr. J. M. Peek should be greatly acknowledged. The work is supported in part by the U.S. Department of Energy, Office of Health and Environmental Research, under Contract No. W-31-109-Eng-38, and Office of Basic Energy Sciences.

[1]M. Inokuti, Rev. Mod. Phys. **43**, 297 (1971); M. Inokuti, Y. Itikawa, and J. E. Turner, *ibid.* **50**, 23 (1978).

[2]J. D. Craggs and H. S. W. Massey, in *Atoms III. Molecules I*, Vol. 37/1 of *Handbuch der Physik*, edited by S. Flügge (Springer, Berlin, 1959), p. 333.

[3]H. Bethe, Ann. Phys. **5**, 325 (1930).

[4]H. Bethe, Z. Phys. **76**, 293 (1932).

[5]M. Inokuti, ANL Report No. ANL-6769 (1963), p. 7 (unpublished).

[6]M. Inokuti, ANL Report No. ANL-7220 (1966), p. 1 (unpublished).

[7](a) S. T. Manson, Phys. Rev. A **3**, 1260 (1971); (b) **5**, 668 (1972); (c) **6**, 1013 (1972); (d) J. H. Miller and S. T. Manson, *ibid.* **29**, 2435 (1984).

[8](a) W. Kołos, Nucleonika **11**, 719 (1960); (b) W. Kołos, H. M. Monkhorst, and K. Szalewicz, J. Chem. Phys. **77**, 1335 (1982); (c) A. Szabo and N. S. Ostlund, Chem. Phys. Lett. **17**, 163 (1972); (d) K. J. Miller, S. R. Mielczarek, and M. Krauss, J. Chem. Phys. **51**, 26 (1969); (e) M. C. Crocker and A. Herzenberg, Mol. Phys. **22**, 483 (1971).

[9]D. R. Bates, K. Ledsham, and A. L. Stewart, Philos. Trans. R. Soc. London Ser. A **246**, 215 (1953).

[10]J. Rankin and W. R. Thorson, J. Comp. Phys. **32**, 437 (1979).

[11]M. Kimura (unpublished).

[12](a) J. M. Peek, Phys. Rev. **134**, 877 (1964); (b) **139**, 1429 (1965); (c) **140**, 11 (1967); (d) **154**, 52 (1967); (e) Phys. Rev. A **10**, 539 (1974).

[13]H. Bethe and R. W. Jackiw, *Intermediate Quantum Mechanics*, 2nd ed. (Benjamin, New York, 1968), p. 304.

[14]S. M. Silverman, Phys. Rev. **111**, 114 (1958).

[15](a) C. Backx, R. R. Tol, G. R. Wright, and M. J. van der Wiel, J. Phys. B **8**, 2050 (1975); (b) K. L. Bell and A. E. Kingston, *ibid.* **8**, L265 (1975).